Integrating technologies for oil spill response in the SW Iberian coast

J. Janeiro [a,*], A. Neves [a], F. Martins [a], P. Relvas [b]

[a] Centro de Investigação Marinha e Ambiental, Universidade do Algarve, Campus de Gambelas, 8005-139 Faro, Portugal
[b] Centro Ciências do Mar, Universidade do Algarve, Campus de Gambelas, 8005-139 Faro, Portugal

Keywords:
Oil spills
Operational modelling
Backtracking
Emergency response
Pollution monitoring
South Iberian coast

A B S T R A C T

An operational oil spill modelling system developed for the SW Iberia Coast is used to investigate the relative importance of the different components and technologies integrating an oil spill monitoring and response structure. A backtrack of a CleanSeaNet oil detection in the region is used to demonstrate the concept. Taking advantage of regional operational products available, the system provides the necessary resolution to go from regional to coastal scales using a downscalling approach, while a multi-grid methodology allows the based oil spill model to span across model domains taking full advantage of the increasing resolution between the model grids. An extensive validation procedure using a multiplicity of sensors, with good spatial and temporal coverage, strengthens the operational system ability to accurately solve coastal scale processes. The model is validated using available trajectories from satellite-tracked drifters. Finally, a methodology is proposed to identifying potential origins for the CleanSeaNet oil detection, by combining model backtrack results with ship trajectories supplied by AIS was developed, including the error estimations found in the backtrack validation.

1. Introduction

Operational Ocean modelling has witnessed a very rapid evolution in recent years. Large scale models covering the major ocean basins have improved their resolution and a new layer of high resolution regional and coastal operational models is now arising, based on those larger models. This evolution is mainly due to improvements in numerical methods and computer performance, motivated by the need of accurate forecasts for research, to support economic activities and for safety and security. The applications of such high-resolution operational models in the field of oil spill pollution are obvious, helping in prevention and during contention, clean-up and recovery phases (e.g. Sotillo et al., 2008; Broström et al., 2011; Janeiro et al., 2014).

Several research studies have focused on the western Iberian oceanography (e.g. Oliveira et al., 2004; Peliz et al., 2005; Relvas et al., 2007; Santos et al., 2011; Pires et al., 2013). With an overall circulation related to all other Eastern Boundary Current System (e.g. Benguela, Humbolt and California), here, the discontinuity imposed by the Mediterranean Sea, together with the seasonality of the large scale atmospheric circulation have a profound impact on the regional oceanography. However, as shown by Álvarez-Salgado et al. (2003), time scales of a few tens of days explain more than 70% of the variability of the coastal alongshore wind stress, a major factor governing the regional coastal circulation. Relvas et al. (2007) presented an extensive review on the physical oceanography of the western Iberia system and characterize the main mesoscale features described for the region. They include a succession of mesoscale structures such as jets, meanders, ubiquitous eddies, upwelling filaments and countercurrents, superimposed on the more stable variations at seasonal timescales as suggested by several authors (e.g. Haynes et al., 1993; Peliz et al., 2002, 2005; Serra and Ambar, 2002; Torres et al., 2003; Relvas and Barton, 2005). Focusing on the southwest coast of the Iberia Peninsula including the south coast and the northern Gulf of Cadiz (Fig. 1), this mesoscale variability is of paramount importance to human coastal activities occurring along a 450 km coastline. Among the activities, the maritime corridor passing between land and the Gorringe Ridge seamount, the Northwest area offshore of the Cape São Vicente, which concentrates shipping routes from the Mediterranean Sea and Southern Hemisphere to Northern Europe, is of special concern due to its high traffic of oil tankers (Janeiro et al., 2012). Based on Automated Identification System (AIS) data, Silveira et al. (2013) characterized the vessels traffic and studied the collision risk inside the Traffic Separation Schemes implemented off the coast of Portugal. From the methodology proposed in the study, and based on one month of AIS data, Silveira et al. (2013) estimated a total of 1766 collision candidates in the entire Portuguese coast. From this total, 355 collision candidates are tankers (Silveira et al., 2013). Based on 36 years of maritime casualties data (between 1971 and 2007), Gouveia et al. (2010) concluded that oil pollution in Portuguese coastal and maritime areas is significant, identifying over 2000 accidents. It is the authors' opinion that this value is underestimated. The lack of surveillance during the timespan of the study could have potentially encouraged illegal discharges that would lead to a significant increase in this number.

* Corresponding author.
E-mail address: jmjaneiro@ualg.pt (J. Janeiro).

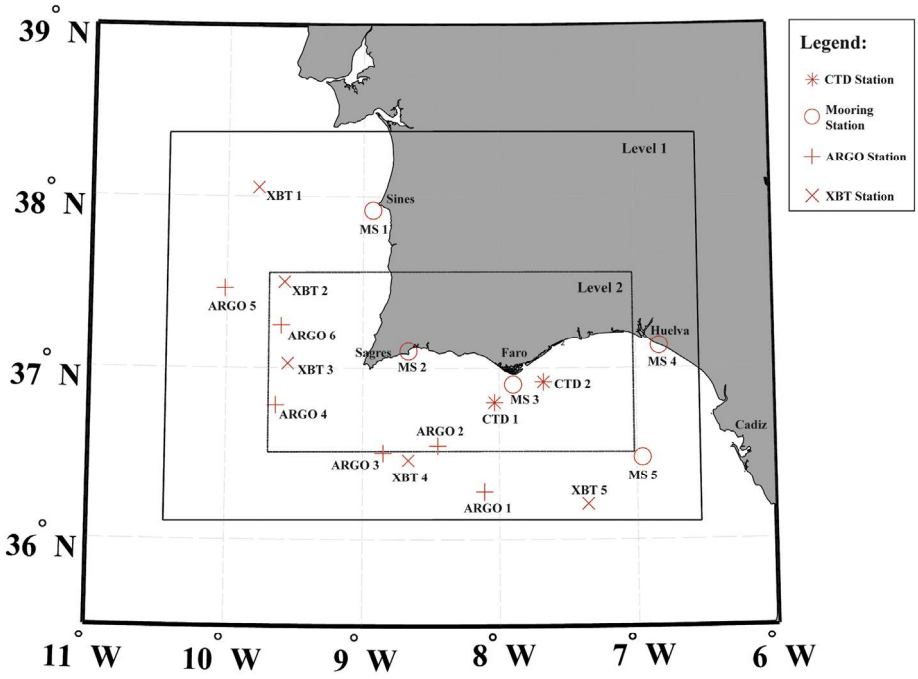

Fig. 1. Geographic grid limits for the two levels comprising SOMA: Level 1 (solid line), Level 2 (dashed line). Distribution of the stations included in SOMA's validation procedure along the SW Iberian coast depicting the instrument type considered.

The local economy is closely linked to the sea, depending mainly from both tourism and fisheries (Janeiro et al., 2012). Environmentally it encompasses several important natural parks, being the most important ones the Ria Formosa Natural Park and the Natural Park of the Sudoeste Algarvio and Costa Vicentina. With a combined area of 92,500 ha and 160 km of coastline, both possess a large biodiversity, a diversity of important natural habitats and act as nursery grounds for several marine species (Bebiano, 1995). So far, the oil spill hazard in the coast of the Algarve has been restricted to maritime transportation. However, eight concessions for offshore oil exploration have been create into the limits of the Algarve coast (DGEG, 2014). These concessions can add an additional oil spill risk for the region in the near future if explorations start.

Since 2007, the EU Member States saw their oil spill surveillance capability amplified with the creation of the European Maritime Safety Agency CleanSeaNet program, which aims at identifying possible marine oil spills through satellite remote sensing. Since the end of 2015, the European Space Agency satellite SENTINEL-1 is responsible to provide this service (EMSA, 2014). The alerts are available within 30 min of the satellite acquiring the image. The national authority then decides how to respond to the alert from CleanSeaNet (EMSA, 2014). The combination of CleaSeaNet oil spill detections and vessel information from SafeSeaNet through AIS with backtracking models from national and regional centres is considered a valuable service to help detection and identification of pollution sources (EMSA, 2014). In fact, tight legislation towards the use of AIS, making it compulsory, and the expansion of the current AIS coverage with the use of satellites, has been an international effort towards increasing the security and safety of maritime transportation.

In this context, an operational response and monitoring modelling system, with the ability to supply sea state and oil spills trajectory forecasts for the Algarve coast is presented in this paper. The goal of this research is to investigate how efficient model downscaling methods can be on backtracking CleanSeaNet oil detections in the marine environment, identifying their possible origins by combining model backtrack results with ships trajectory supplied by AIS. The article is structured as follows: (1) the operational system and downscaling methodology will be described followed by the validation results, obtained against in-situ measurements from several type of sensors; (2) the Lagrangian validation of the system and its capability to backtrack an oil spill was tested in a real event; finally (3) the main results are discussed and conclusions drawn regarding the model implementation and ability to respond to oil pollution emergencies in the region.

2. Operational model

The operational system proposed, hereby SOMA (Algarve Operational Modelling and Monitoring System), encompasses a hydrodynamic model and an oil spill model. The system is based on the MOHID water modelling system (Martins et al., 2001; Balseiro et al., 2003; Leitão et al., 2005) due to its architecture, which allows the use of several modules (e.g. Hydrodynamic, Water Properties, Oil Properties), communicating in real time during a simulation making it a suitable and robust tool for this kind of downscaling methodologies (Janeiro et al., 2014). It encompasses two grid levels of increasing resolution (Fig. 1) built using bathymetric data retrieved from the European Marine Observation and Data Network (EMODNET - http://www.emodnet.eu). Level 1 (Fig. 1) is a three-dimensional model, with a constant horizontal resolution of 3 km, 11 sigma layers in the first 20 m depth and a resolution of 75 cm at the surface layer. From the 20 m to the bottom 35 unevenly spaced Z coordinate levels vertically discretize the model. This hybrid type of vertical discretization is possible due to MOHID's generic vertical coordinate approach. A time discretization of 30 s is used with this mesh. At the boundary, a Blumberg and Kantha (1985) condition is applied to the water level and a Flow Relaxation Scheme (FRS) (Martinsen and Engedahl, 1987) is used for velocity, salinity and temperature. This allows a smooth forcing of the model and a weighting of internal and external solution to prevent an overshoot of the dynamic equilibrium. In the outer grid cells a sponge layer was applied to attenuate reflected spurious baroclinic flow oscillations.

Level 2 (Fig. 1) is a three-dimensional model with a regular 1 km spatial resolution grid covering the Algarve coast. It has the same vertical resolution of Level 1 and a time discretization of 15 s. The communication between Levels 1 and 2 is made using FRS to relax the zonal and meridional horizontal velocity components, through an eight cells band adjacent to the lateral boundary. The use of these boundary conditions

is consistent with the conclusions of Blayo and Debreu (2005) that considered relaxation methods to be suitable boundary conditions, giving reliable results in actual applications. Turbulent diffusion coefficients are computed in MOHID using its embedded version of the General Ocean Turbulence Model (GOTM) (Buchard et al., 1999; Umlaut and Burchard, 2005). The mixing-length scale parameterization proposed by Canuto et al. (2001) is used. Boundary conditions for temperature, salinity, tide and current velocities are supplied by the Portuguese Coast Operational Modelling System (PCOMS) (Campuzano et al., 2014; Mateus et al., 2012; Ascione Kenov et al., 2014). Atmospheric forcing conditions are supplied by the regional weather forecasting system SKIRON, developed for operational use at the Helenic National Meteorological Service (Kallos, 1997; Papadopoulos et al., 2001). It provides hourly data of wind velocity components, air temperature, specific humidity, total cloud cover, sea level pressure, total precipitation, upward and downward long wave flux, evaporation, latent heat flux and sensible heat flux at a resolution of 5 km. SKIRON results are used in the operational system as atmospheric forcing fields for the hydrodynamic models.

2.1. Hydrodynamic model validation

SOMA hydrodynamic validation was accomplished using several data sources from different data providers. The validation dataset included data from tide gauges, moored buoys, vertical profiles (CTD, XBT, ARGOS), ADCP, HF Radars and remote sensing, spanning several years (2009–2014). To evaluate the model performance absolute and relative error metrics were considered, as suggested by O'Donncha et al. (2015). The Root Mean Square Deviation error (RMSD), mean BIAS and Willmott (1981) Model Skill Score (MSS) where applied:

$$RMSD = \sqrt{\frac{\sum_{i=1}^{n} (x_{model} - x_{obs})^2}{n}} \quad (1)$$

$$BIAS = \frac{\sum_{i=1}^{n} (x_{obs} - x_{model})}{n} \quad (2)$$

$$MSS = 1 - \frac{\sum_{i=1}^{n} (x_{model} - x_{obs})^2}{\sum_{i=1}^{n} (|x_{model} - \overline{x}_{obs}| + |x_{obs} - \overline{x}_{obs}|)^2} \quad (3)$$

x_{model}, x_{obs} are the model predicted and observed values respectively, while $\overline{x}_{obs}$ is the mean of the observed values. While the RMSD and mean BIAS are dimensional variables providing an absolute measurement of the error between the datasets, the MSS is non-dimensional, providing a deeper insight into the predictive abilities by overcoming the sensitivity of the correlation statistics to differences in the predicted mean and variances (O'Donncha et al., 2015). MSS varies between 0 (total disagreement between model and observations) and 1 (total agreement between model and observations).

Sea Surface Temperature (SST) was validated using remote sensing data from both MODIS Aqua and METOP-A satellites. MODIS dataset, consisting of 470 MODIS binned 4 km images, was retrieved from NASA's Ocean colour webpage (NASA, 2014). METOP-A dataset comprised approximately 7800 daily world SST images with 1 km resolution and was retrieved from OSI SAF webpage (OSI SAF, 2013) for the period of interest. Based on the flagging methodology only images with "good data" where considered. SOMA SST was then validated for a five days' period (30/08–04/09/2013) which encompassed a relaxation of the upwelling favorable winds and the establishment of a warm countercurrent, progressing, in the inner shelf, from the Gulf of Cádiz to Cape São Vicente where it turned poleward. This circulation pattern has been described by several authors (Relvas and Barton, 2005; García-Lafuente et al., 2006; Teles-Machado et al., 2007) being considered a distinctive feature of the Western Iberia inner shelf circulation. By using a combination of images from both METOP-A and MODIS satellites a total of 21 good quality SST images covered the event providing a useful high-resolution spatial and temporal dataset for validation. For each satellite image, the difference between model and satellite was computed and results were quantitatively accessed through RMSD error and correlation coefficient (R) estimated for each available date by means of a linear regression. This evaluation was done for both grid levels of SOMA. Fig. 2 depicted the comparison obtained between SOMA Level 1 and a METOP-A image for day 01/09/2013. Higher differences in SST between model and observations occur in regions were colder upwelled waters are present (between 1 and 2 °C). Differences in SST are also visible in the region of the Gulf of Cádiz although to a lower extend. The statistical evaluation of this comparison provided values of −0.26 °C, 1.08 °C and 0.827 for, respectively, the mean BIAS, RMSD error and R.

Due to the number and quality of available satellite images, this countercurrent event was also analyzed in what regards SOMA's ability to reproduce its temporal evolution in each level of the operational system. This was achieved by computing both RMSD and R between satellite images and model results throughout the event. Fig. 3 illustrates the results obtained. Results show a good ability from SOMA to reproduce the evolution of the countercurrent event. Level 1, although presenting lower RMSD errors and higher R values in the first days of the event when comparing with Level 2, shows an increase in error, with resulting decrease in correlation, as the event evolves in time.

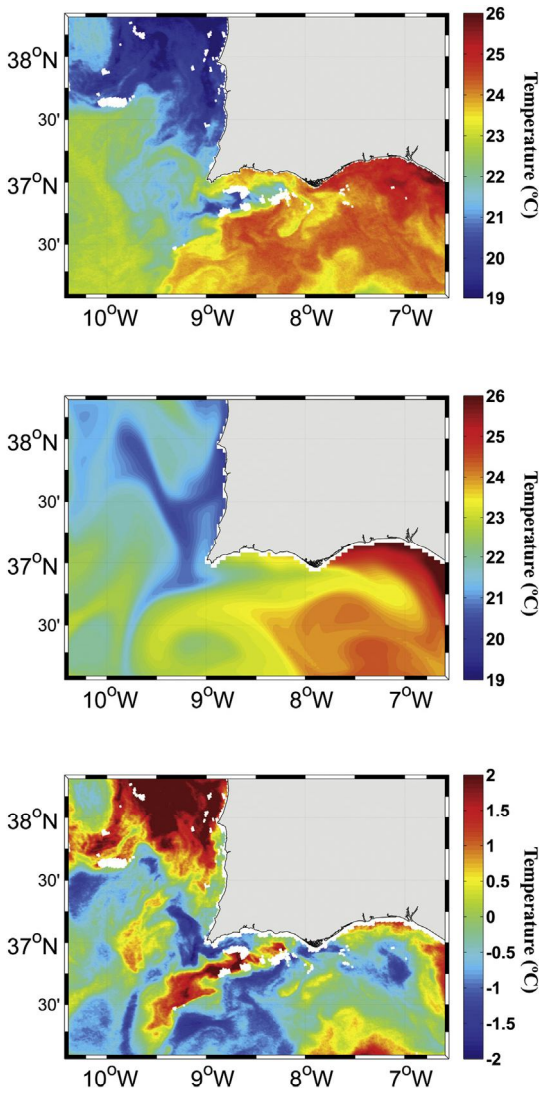

Fig. 2. SST validation results for day 01/092013. Respectively, from top to bottom: METOP-A satellite image, SOMA Level 1 and difference between model and observations.

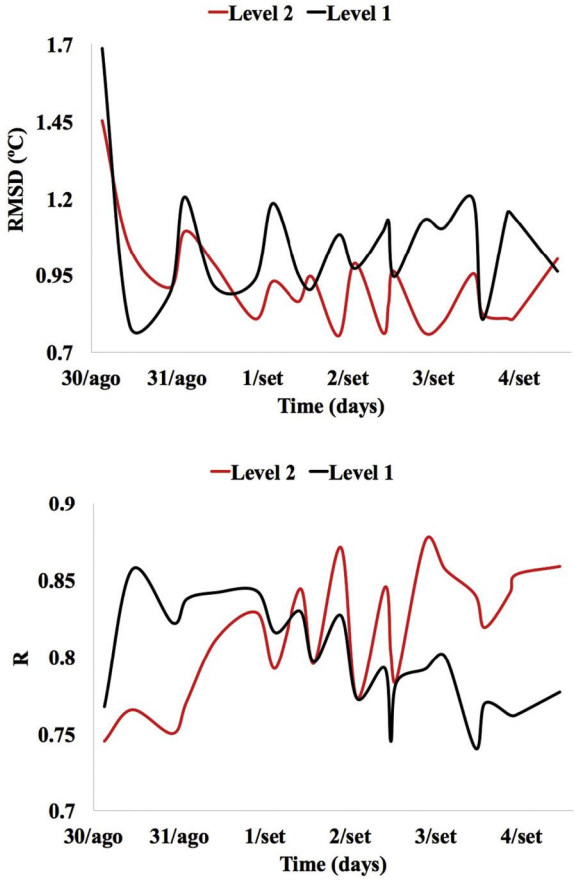

Fig. 3. Temporal evolution of the RMSD error and R between model results and satellite observations for the countercurrent event. Results from SOMA Level 2 are shown in red, results for Level 1 are shown in black. (For interpretation of the references to colour in this figure legend, the reader is referred to the web version of this article.)

Observations from five moored stations where used to validate the hydrodynamic model: two tidal gauges in Lagos and Huelva (stations MS 2 and MS 4); two wave buoys: off the coast of Sines a Datawell MK2 (MS 1) and off the coast of Faro a Datawell MK3 (MS 3); a multi-parameter ocean buoy SeaWatch Directional Ocean-Met in the Gulf of Cádiz (MS 5). These datasets were provided by the Portuguese Instituto Hidrográfico (wave buoys from Sines and Faro and Lagos tidal gauge) and from the Coriolis project and programmes contributing to it (http://www.coriolis.eu.org). The distribution of the sensors in the model domain is presented in Fig. 1. Due to data availability two different periods were considered in our analysis. The tidal observations from MS 2 and MS 4 tide stations were compared with model results for a twenty-day long period in May 2012, while the validation using MS 1, MS 3 and MS 5 stations was done, for the same amount of days, in October 2013. Stations MS 1 and 3, were subject to a post-processing step due to the high frequency of data available (every 10 min). In this post-processing both time series were filtered to eliminate frequencies above tide by means of a Cosine-Lanczos low-pass filter with half power point at 6 h spanning 50 h. The results obtained for the time series analysis are summarized Fig. 4.

Considering the MSS obtained for the time series comparisons, a good level of agreement between observations and model predictions was accomplished. Tide validation was successfully achieved with RMSD errors of 13 cm (MS 2) and 10 cm (MS 4) and MSS of 0.99 for both stations. Surface temperature was validated in three moored stations covering both south and southwest coasts. Results show a distinction in the models ability to reproduce the surface temperature evolution between both coasts. A RMSD error of 0.98 °C was found for station MS 1, contrasting with the 0.5 °C and 0.36 °C for station MS 3 and MS 5, while MSS varied from 0.63 (station MS 1) and 0.96 (stations MS 3 and MS 5). Salinity at station MS 5 with a RMSD error of 0.21 was the property presenting the lowest MSS value (0.31). SOMA's ability to reproduce vertical variations in temperature, salinity, and density was evaluated by using profiles available for the study area. Profiles from ARGO buoys, expendable bathythermographs (XBT's) and CTD where employed. Due to data availability and to ensure a good geographical coverage on both model levels', the data spanned between the years

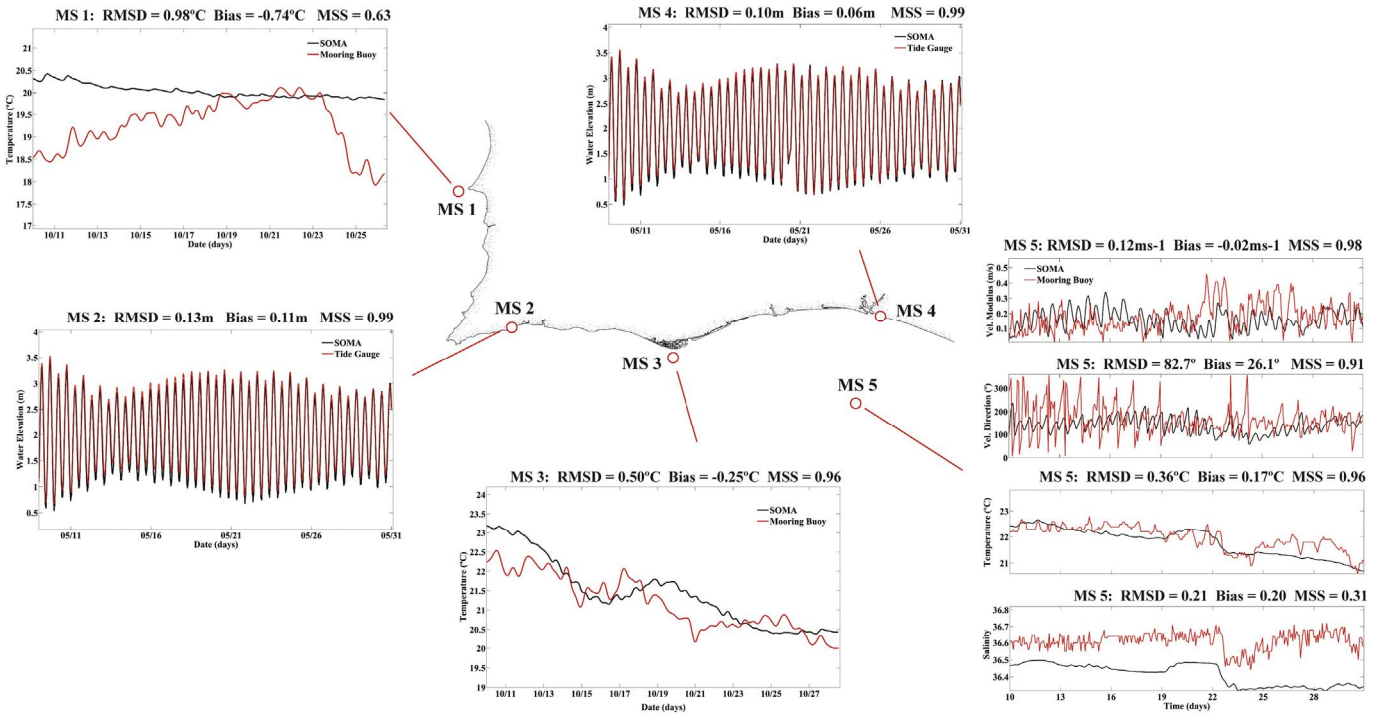

Fig. 4. Validation of SOMA surface properties (temperature, salinity, water elevation, velocity modulus and velocity direction) using time series from moored stations available in the region. The respective error estimations are provided on top of each plot by means of the RMSD error, mean BIAS and MSS.

of 2011, 2012 and 2013. In Fig. 1 the spatial distribution of the stations used is indicated. ARGO and XBT profiles were collected and made freely available by the Coriolis project for 2013 and 2011 respectively. Profile depths ranged the 1000 m in each station. CTD profiles and were carried out during September 2012 in the scope of the EU programme Eurofleets using a SeaBird SBE 911plus CTD. Fig. 5 illustrates the

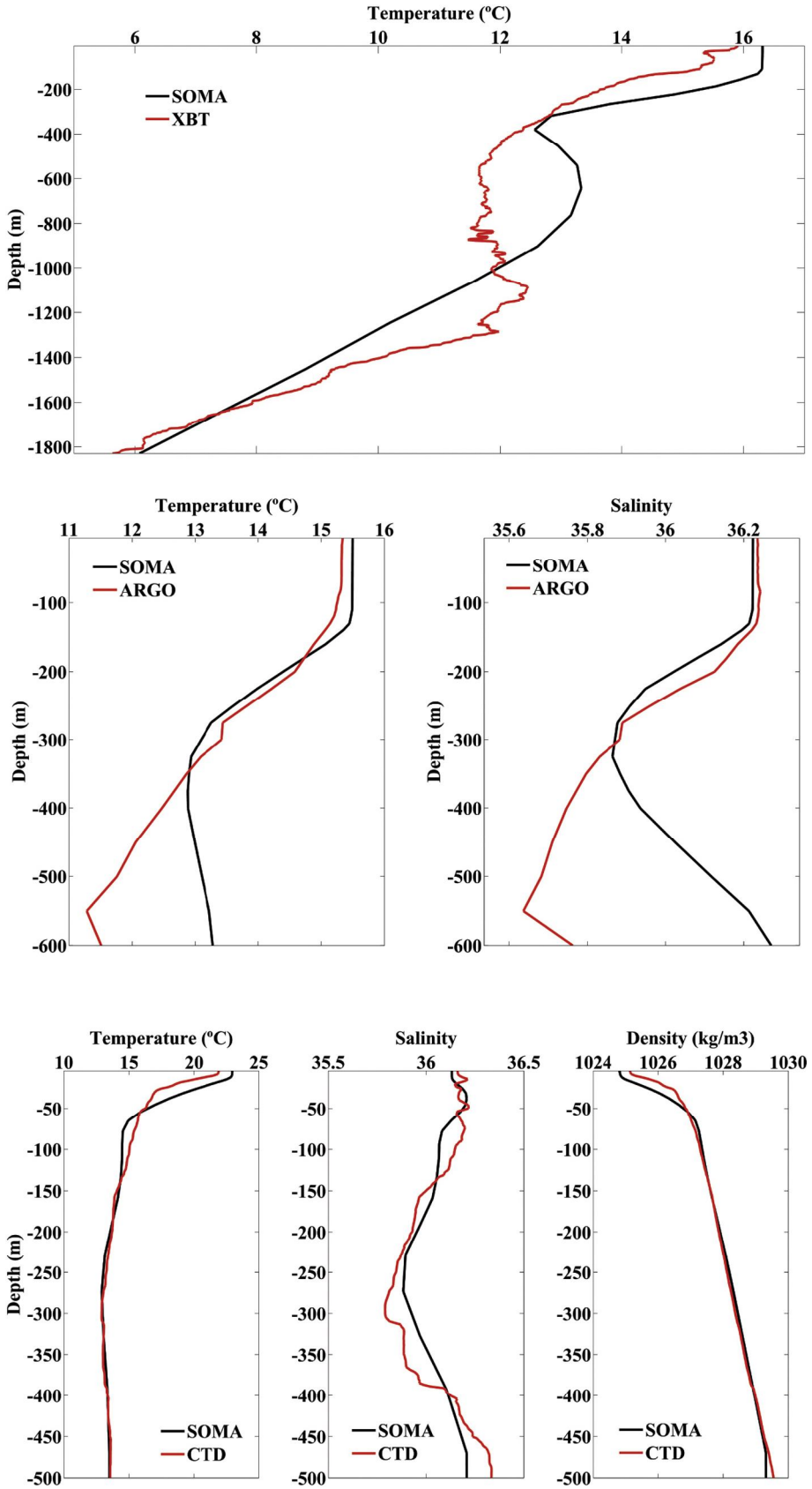

Fig. 5. SOMA validation of temperature and salinity through vertical profiles at three stations. From top to bottom: XBT 1; ARGO 5 and CTD 1.

Table 1
Estimated errors and MSS for the validation of SOMA's vertical distribution of temperature, salinity and density.

Station	Property	RMSD	Bias	MSS
ARGO 1	Temperature	0.63 °C	−0.35 °C	0.99
	Salinity	0.17	−0.04	0.99
ARGO 2	Temperature	0.72 °C	0.17 °C	0.99
	Salinity	0.25	0.03	0.99
ARGO 3	Temperature	0.61 °C	0.1 °C	0.99
	Salinity	0.24	0.02	0.99
ARGO 4	Temperature	1.21 °C	0.02 °C	1.00
	Salinity	0.38	−0.05	0.98
ARGO 5	Temperature	0.53 °C	−0.26 °C	0.98
	Salinity	0.15	−0.04	0.98
ARGO 6	Temperature	0.62 °C	−0.34 °C	0.97
	Salinity	0.17	−0.06	0.95
XBT 1	Temperature	1.06 °C	−0.24 °C	0.99
XBT 2	Temperature	0.95 °C	0.17 °C	0.99
XBT 3	Temperature	0.90 °C	0.57 °C	0.94
XBT 4	Temperature	1.61 °C	1.01 °C	0.95
XBT 5	Temperature	0.57 °C	−0.10 °C	0.99
CTD 1	Temperature	0.64 °C	0.17 °C	1.00
	Salinity	0.08	−0.005	1.00
	Density	0.18 kg/m^3	0.04 kg/m^3	1.00
CTD 2	Temperature	0.64 °C	0.23 °C	0.99
	Salinity	0.14	0.04	0.96
	Density	0.15 kg/m^3	0.02 kg/m^3	0.99

validation results obtained for some vertical profiles along the south and southwest coasts. Estimated errors between model results and observations are summarized in Table 1 for all profiles considered in this study.

A good agreement between model results and vertical profiles was achieve throughout the model domain and in both grid levels, with MSS values very close to 1 (perfect agreement). Results highlight the suitability of the vertical domain implemented. SOMA's current velocities were validated in depth (ADCP), at the surface (HF Radar) and as a time series at station MS 5. An ADCP transect carried out during September 2012 in the scope of the EU programme Eurofleets using a hull mounted RDI OS 75 kHz ADCP was used to validate the model current velocity in depth, with results presented in Fig. 6. The ADCP data was pre-processed using the CODAS (Common Ocean Data Access System) processing software (http://currents.soest.hawaii.edu/docs/doc/). Two ADCP depths (35 and 105 m) were chosen for the comparison, with model results being interpolated for the time of the ADCP transect and each of the depths considered. The RMSD error and MSS were used to quantitatively access the results.

Results achieved reveal SOMA's good ability to reproduce the currents observed at the considered depths. For both current velocity and direction, errors found at 35 m depth (RMSD of 0.08 m/s and 74.3°) presenting MSS values of 0.97 for the current velocity and 0.49 for the direction. At 105 m depth results found for the MSS where 0.81 (current velocity) and 0.93 (current direction) with RMSD errors of 0.06 m/s and 115°. Surface currents were validated using High-Frequency Radar (HFR) technology provided by the Portuguese Instituto Hidrográfico (IH) and the Spanish Puertos del Estado which, since 2013, are implementing a joined network of HFR Codar SeaSonde antennas to monitor sea surface currents and waves in the Gibraltar Strait and at the boundary area between Spain and Portugal (Mazagon and Monte Gordo). This HFR network provides hourly data with a maximum range of 75 km and a resolution of 1.3 km. On month (October 2014) of hourly HFR observations were used to validate SOMA surface currents. From available dataset, few observations provided enough spatial coverage for a meaningful statistical comparison with model results, thus in Fig. 7 a snapshot for the 04/10/2014 illustrates the comparisons between HFR and both SOMA levels. For this date, results for Level 1 (top panel) show a good agreement between the SOMA surface currents and HFR observations particularly near the eastern coast. Quantitatively, results were evaluated by mean of the RMSD error and MSS for the meridional and zonal velocity components. In Level 1, RMSD errors of 0.12 m/s and 0.10 m/s were found, respectively, for the zonal and meridional components of the velocity, with MSS being 0.97 and 0.70. Results obtained for Level 2 (bottom panel) are in close agreement with what was found for Level 1, but with an increase in the surface current velocity in the east coast. This increase in velocity, mainly explained due to differences in bathymetry resolution, slightly improves the comparison with observations. In this level, MSS values of 0.99 and 0.66 were found for the zonal and meridional velocity component with RMSD error being 0.11 m/s for both components.

Finally, a twenty-day surface current velocity and direction time series recorded at station MS 5 was also used in SOMA hydrodynamic validation, with results presented in Fig. 4. For this time period a good comparison was achieved between model and observations, with RMSD errors of 0.12 m/s and 82.7° and MSS values of 0.98 and 0.91 for, respectively, current velocity and direction.

3. Backtracking CleanSeaNet detection

3.1. Lagrangian model validation

To simulate the oil spill trajectories and weathering processes, the multi-mesh Lagrangian model (Fernandes et al., 2013) implemented in MOHID is used together with its oil weathering model (Janeiro et

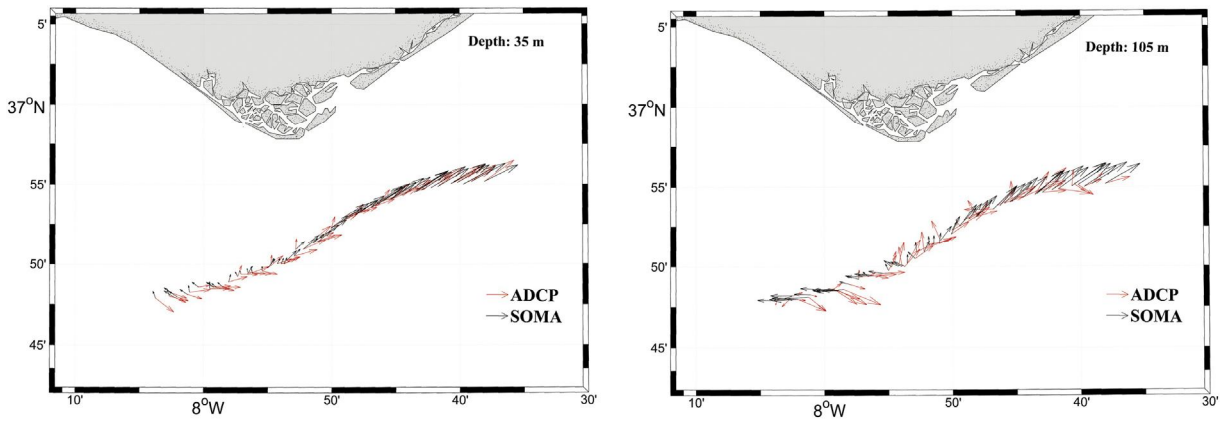

Fig. 6. Model validation against an ADCP transect obtained during the EU programme Eurofleets. ADCP velocity (red arrows) was computed for the 35 m and 105 m depth and used to validate SOMA results (black arrows) interpolated for the time and depth of the ADCP transect. (For interpretation of the references to colour in this figure legend, the reader is referred to the web version of this article.)

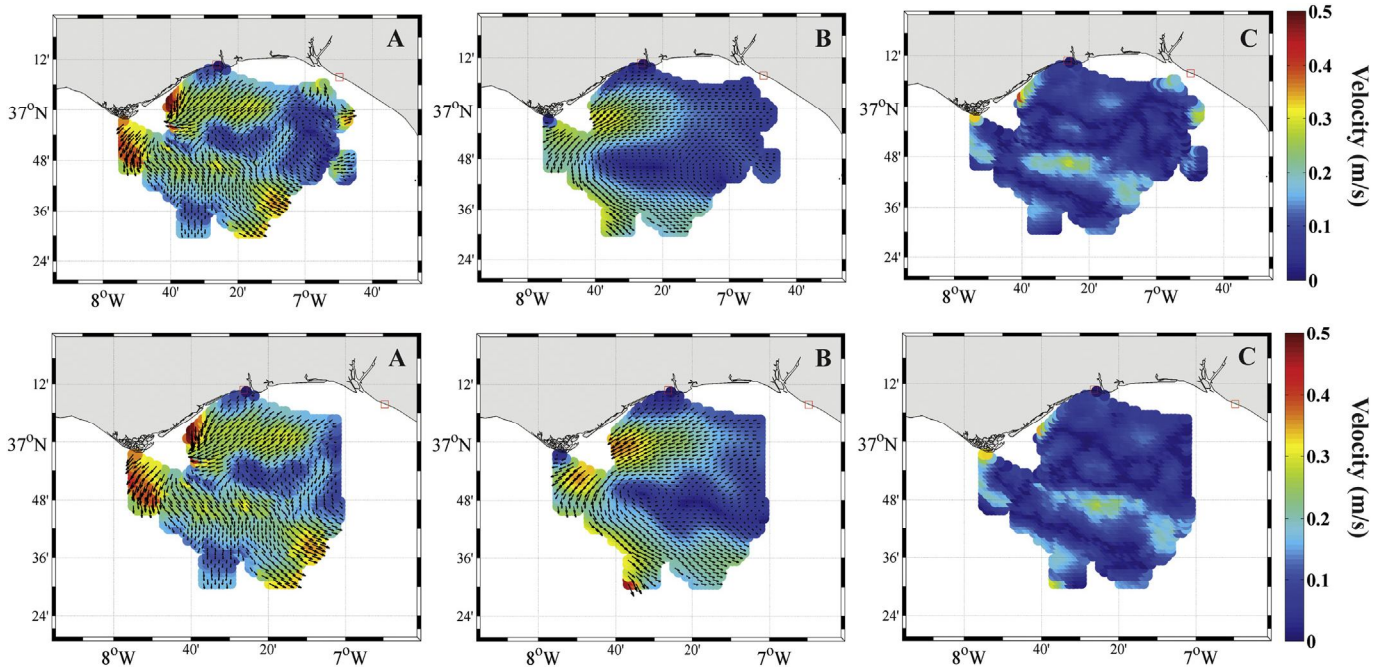

Fig. 7. Validation of model surface currents, for both Level 1 (top panel) and Level 2 (bottom panel), against HFR observations in the South Iberian coast. HFR observations (A) are compared with model results interpolated to the HFR grid (B) with the RMSD error for the comparison being represented in C. The location of the HFR antennas is represented as a red rectangle. (For interpretation of the references to colour in this figure legend, the reader is referred to the web version of this article.)

al., 2008). Here, the spatial evolution of the particles is computed integrating the definition of velocity:

$$\frac{dx_i}{dt} = U_i(x_i, t) \tag{4}$$

where

$$U_i = u_{1i} + u_{2i} + u_{3i} + u_{4i} + u_{5i} \tag{5}$$

u_{1i} is the hydrodynamic velocity. MOHID multi-mesh approach ensures that the Lagrangian model uses, from the available model levels, the best hydrodynamics to force the Lagrangian tracers. MOHID integrative architecture allows that both hydrodynamic model and Lagrangian model run simultaneously, sharing the same code, with further advantages in the accuracy of the computed trajectories, as suggested by Janeiro et al. (2014). u_{2i} is the drift velocity due to the wind. u_{3i} is the velocity due to the spreading of oil (which is calculated in the oil module and updated by the module). u_{4i} is the random velocity due to diffusive transport (Allen, 1982) and finally u_{5i} is the stokes drift (Fernandes et al., 2013). The stokes drift will not be considered in this study. While identified as a relevant mechanism affecting the trajectory of oil spills (Janeiro et al., 2014), at this stage, there was no regional product implemented to supply wave data to the operational system. This will change in the near future as work is being done to implement a dedicated wave model in the region based on SWAN (Simulating WAves Nearshore model).

MOHID oil module (Fernandes, 2001; Janeiro et al., 2008) include the physical processes of the oil (density and viscosity) and the weathering processes (e.g. evaporation, dispersion, emulsification, dissolution), updating the module in each timestep. Although oil weathering processes are included in MOHID oil module, these processes were not considered here, focusing this study on trajectory evolution of oil spills. This was done due to data availability to validate the Oil Module. Information regarding the evolution of a real oil spill is needed and there is no data available for the study region that might be used in this regard. Since satellite-tracked drifters were the available data for validation, oil dispersion is the only oil weathering process suitable to be validated using this dataset. Nonetheless, drifter data was sparse in time and limited in number of drifters, for each time period, to allow a proper validation of the dispersion.

Drifter buoys have been applied by several authors (e.g. Caballero et al., 2008; Verjovkina et al., 2010; Zodiatis et al., 2012; Dominicis et al., 2013a; Janeiro et al., 2014) to validate oil spill models, as model simulated drifter trajectories can be directly compared with independent drifter experiments (Barron et al., 2007; Thompson, 2003). In this research, 5 drifting buoys trajectories, drogued at a depth of 15 m, were used to validate the model. The data makes part of the Surface Drifting Program (SVP) and was made available by the Coriolis project, covering the period from 2011 till 2014. Model drifters were released in the location where satellite-tracked drifters were observed, and their separation distance is used as a direct measurement of the trajectory model skill. The buoys positions were compared with the simulated trajectory of 200 particles during 48 h.

The number of Lagrangian particles was selected considering the computational cost of each simulation. Although in the work of Dominicis et al. (2013a, 2013b) a methodology is presented to determine the of range of particles that better represent oil concentrations in oil spill simulations, this work focused on the trajectory of the spill rather than its physical and chemical properties, thus the number of particles is not relevant (Zodiatis et al., 2012). The total release may be envisaged as a particle "cloud" which represents the probability of the buoy position, being thus described as a "probability cloud". In this approach a particle cannot be subdivided and is unable to interact with other particles. The multi-mesh approach ensures that the high-resolution hydrodynamics (Level 2) is used whenever the particles move into its geographical boundaries. Turbulent diffusion coefficients were adjusted to better represent the drifters' trajectories and oil weathering processes were not considered in the simulations since comparison is made with drifters. To compare the buoy trajectory with the model results (Fig. 8), the centre of mass of the particles outputted by the model was calculated according to the method proposed by Janeiro et al. (2014).

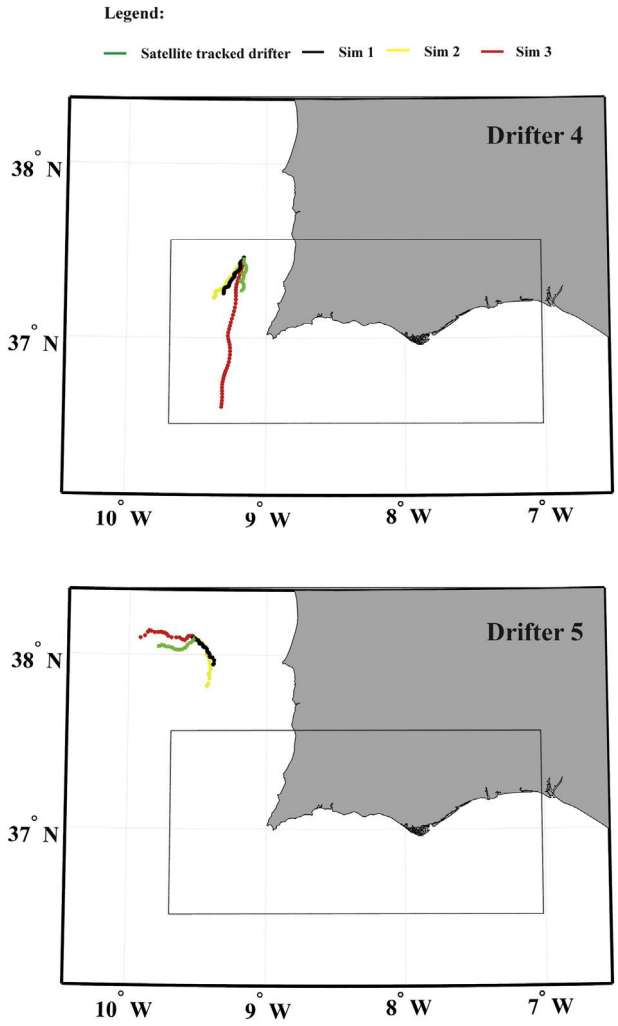

Fig. 8. Lagrangian model validation. Trajectories for satellite-tracked drifters (green) are compared with the center of mass of the cloud of particles for: Sim 1 corresponds to the release of 200 particles at 15 m depth (black), Sim 2 corresponds to the release of 200 particles at the surface (yellow), Sim 3 corresponds to the release of 200 particles at the surface but considering 3% of the wind velocity affecting the particles (red). The figure geographic limits match those of Level1 and Level2 region is presented with the dashed rectangle. (For interpretation of the references to colour in this figure legend, the reader is referred to the web version of this article.)

The errors between buoy and simulated trajectories were estimated using the trajectory-based non-dimensional index proposed by Liu and Weisberg (2011):

$$s = \sum_{i=1}^{N} d_i / \sum_{i=1}^{N} l_{oi} \tag{6}$$

d_i is the separation distance between modelled and observed endpoints of the trajectories at time step i after start, $l_{oi}$is the length of the observed trajectory, and N is the total number of time steps. A total agreement is reflected by an s value equal to zero. As a first approach, a model scenario assuming the release of 200 particles at 15 m depth (anchor depth of the drifters) was simulated (Sim 1). The trajectories results are presented in Fig. 8 while Table 2 show the s index values obtained for the simulations. With this approach four of the five drifters show comparisons with high s index values, the only exception is Drifter 4 ($s = 0.45$). This fact was also reported by Janeiro et al. (2014) with the authors suggesting several factors that might explain the discrepancies found. Among them, the change in anchor depth due to deterioration of the drifter's sock and the fact the velocity affecting the drifter is an integration of the current velocities from the surface to the anchor depth, along the connecting cable, considering that velocities in depth will have more weight than the ones at the surface due to the drifter's sock, rather than the current velocity at the drifter's depth.

Table 2
Values obtained for s index and distance model-buoy after 24 h considering the five drifters studied and three simulation scenarios: Sim 1 – Depth of the particles equal to depth of the drifter sock (15 m); Sim 2 – particles imposed at the surface: Sim 3 – particles imposed at the surface plus a 3% wind velocity.

Scenarios	s Index/distance model-buoy (24 h)				
	Drifter 1	Drifter 2	Drifter 3	Drifter 4	Drifter 5
Sim 1	0.82/31 km	1.08/18 km	0.96/39 km	0.45/5 km	1.16/9 km
Sim 2	0.76/31 km	0.48/9 km	0.86/36 km	0.69/8 km	1.30/12 km
Sim 3	0.76/24 km	0.48/9 km	0.86/36 km	2.90/40 km	0.48/6 km

To address these problems a simulation with the Lagrangian particles located at the surface was conducted (Sim 2). The results obtained show that the trajectories of the centre of mass at the surface or at 15 m didn't have a significant change, in fact in some cases (Drifters 3 and 5) both trajectories were in the opposite direction of the drifters'. A final simulation (Sim 3) was conducted combining the surface scenario with 3% of the wind velocity affecting the particles. Although the results for the s index (Table 2) didn't show substantial improvements from the surface scenario (only Drifter 5 presenting a lower s index value) the wind correction seem to affect the trajectories of the particles in the model, which now follow the observed ones. The wind correction also induced an overestimation of the velocities affecting the particles, which also explain the s values obtained, as detailed further on.

Although the multi-mesh approach implemented in MOHID Lagrangian model allow the use of the best hydrodynamic available to force the particles, the relative performance of both levels of SOMA in reproducing drifters' trajectory was accessed by re-run Drifter 4 (the only drifter with a trajectory falling completely in Level 2) Sim 1 scenario using only Level 1 hydrodynamics. The distance model-buoy after 24 h was 8 km and the s index found for the entire simulation was 0.64. These results differ for the ones found for Level 2 which are, respectively, 5 km and 0.45, showing the improvements in considering the high-resolution Level 2 in SOMA.

3.2. Backtracking CleanSeaNet detection

During oil pollution accidents, backtracking methods allow to simulate a spill back in time from its detection to a potential origin point. This feature is useful to detect likely illegal discharges and potential polluters. With the objective of backtracking a CleanSeaNet detection in the study area, MOHID model was run in backtracking mode (Fernandes et al., 2013). Using scenario Sim 2, the one presenting lower s index values when averaging all drifters (Table 2). To validate and quantify the trajectory errors associated to the backtracking method 48 h backtracking simulations where conducted for the five satellite-tracked drifters. Again, oil-weathering processes were not considered. The temporal evolution of d_i was computed for the entire backtracking simulations in three hours intervals. This time interval was used to normalize the drifters sampling frequency. Subsequently, the $d_i$values obtained were averaged over the total number of buoys following the procedure described in Abascal et al. (2012):

$$d_m(t) = \frac{1}{N_b} \sum_{i=1}^{N_b} d(t)_i \tag{7}$$

where d_m is the averaged separation distance, t is the time and N_b is the number of buoys. Fig. 9 illustrates the evolution of d_m for the backtracking simulation timespan.

This methodology concurs with the proposed by Price et al. (2006) and later by Abascal et al. (2009), who found the separation distance between model and satellite-tracked drifter trajectories during short time scales, a useful way of assessing applications related to oil spill

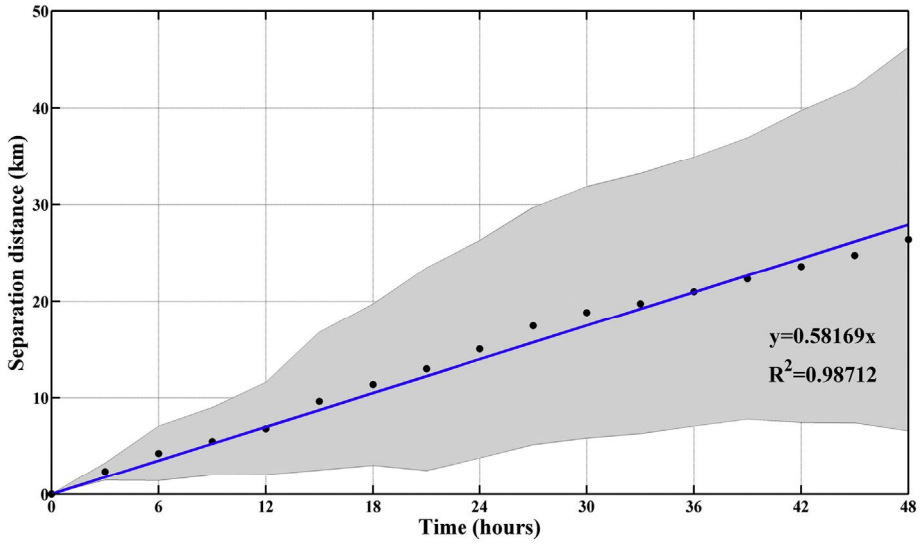

Fig. 9. Evolution of d_m for the backtracking simulation timespan. The mean and standard deviation values are presented with black dots and grey area, respectively.

trajectories. From Fig. 9 it is possible to perceive the increasing uncertainty in the backtracking results along the 48 h simulation timespan. In practical terms, the results show that in the event of a spill detection, if we backtrack the spill evolution 48 h, the estimated area of search to find the spill would have a radius of approximately 26.4 ± 19.8 km from the position given by the backtrack simulation. This value decreases to 15 ± 11.3 km if a 24 h backtrack is used and to 6.7 ± 4.3 km for a 12 h backtrack.

Following the validation procedure, SOMA was used in hindcast mode to backtrack a CleanSeaNet detection in the study area (approximately 65 km southeast Sagres on the 20th of September 2012) during 48 h. As previously mentioned, the CleanSeaNet provide the detection of possible oil spills, in situ verification is always required. For the CleanSeanNet detection considered, which presented a medium confidence level, there was no in situ confirmation of an oil spill by the Portuguese authorities. Nevertheless, due to scientific nature of this study the detection was considered suitable to validate the methods described further.

To identify possible sources for this potential pollution event, model backtracked trajectories where combined with Automatic Identification System (AIS) positions of the ships nearby. The Centre of Marine Sciences (CCMAR) supplied the AIS data. To include the errors obtained in the backtrack validation a simple linear regression was computed for the $d_m$results (Fig. 9). From this regression d_m values for 12, 24, 36 and 48 h where found and used as search radius to find ships positions and their correspondent identification number (MMSI) from the AIS database. The MMSI identified where then matched against freely available web AIS service providers, and information on the type of ship was used to classify the detections in six groups (oil tankers, general cargo, fishing, passengers, sailing, unknown). From the identified groups, only oil tankers and general cargo boats are presented due to the size of the potential spill observed. Fig. 10 summarizes the results obtained. From a total of 6 detections only 4 where considered, being one tanker (red trajectory) and three general cargo ships (brown trajectories). The filled dots symbolize the ship location upon detection, with its trajectory from the AIS being represented with a line.

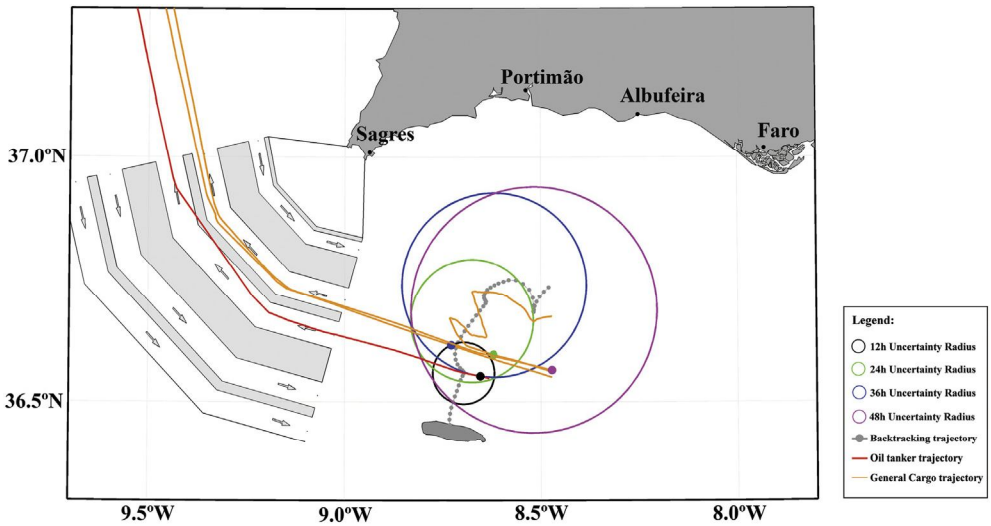

Fig. 10. Backtracking results (grey dots) for a CleanSeaNet detection (grey polygon) in the southern Portuguese coast. The circles correspond to the search area used to filter the AIS positions, increasing for a 12 (black), 24 (green), 36 (blue) and 48 (magenta) hour periods in accordance with Fig. 9. Filled dots represent the ship position in the time frame of the detection, while lines represent ships trajectories from AIS colour coded, by type of ship, as follows: tankers (red), general cargo (brown). (For interpretation of the references to colour in this figure legend, the reader is referred to the web version of this article.)

4. Discussion

4.1. Hydrodynamic model validation

Based on the results obtained, in the overall, SOMA hydrodynamic component was considered validated. This is strengthened by the extensive validation procedure, with both a good spatial and temporal coverage (covering conveniently both model grids) while spread along a multiplicity of sensors. Although MSS values found are in general close to 1 (perfect agreement), differences between model and observations were found and will be discussed further. These differences can be due to a multiplicity of factors, as pointed out by Price and Bush (2004), including numerical errors (e.g. forcing fields, model implementations and boundary conditions methods) and observation errors (e.g. satellite-tracked drifters may contain location errors due to their long period at the sea).

Remote sensing observations provide a good tool to validate regional and coastal models, especially in regions characterized by strong temperature gradients like the study area. In terms of SST, the southwest and south coast are two well-distinguished areas (Peliz et al., 2009; Relvas et al., 2007). This is clear from satellite images but also from in situ observations. Looking at the results obtained, differences in SST exist between satellite images and model results, nonetheless, in general the model represents to a good extend the countercurrent event. When looking at evolution of the event in the satellite images a lag in the model ability to reproduce the countercurrent event is noticeable and illustrated in Fig. 3. When compared with the satellite images, in the first day, both SOMA Levels present a high RMSD error and lower R since there was no relaxation of the upwelling in the model and the countercurrent event was still not developed. As the intensification of the upwelling occurs in the SST observations near Sines, the agreement between Level 1 and observations increases when compared with Level 2. While SOMA Level 1 grid limits allow to cover this upwelling region, the geographic limits of its high-resolution Level 2 don't extend so far north and westwards. From 01/09 onwards, SOMA starts to develop the countercurrent event (with the associated relaxation of the upwelling in the west coast) noticeable in Fig. 3 by the increasing of R in Level 2. The countercurrent event also develops in Level 1, but the differences between model and observations, predominantly in the upwelling region near Sines outside Level 2 grid limits, lower the comparison. Two main reasons may explain this lag: 1) errors both atmospheric and hydrodynamic forcing fields; 2) SOMA vertical resolution and mixing parametrizations, which influence the ocean upper layer response time to the wind forcing in the model. While SOMA vertical resolution and mixing parametrizations, accessed during the validation with vertical profiles with good results, performs adequately, to minimize errors in the forcing conditions, the inclusion in SOMA of new forcing providers, already including recent advances in data assimilation and improved resolutions, is being considered.

Time series observations provide a good insight on the model ability to correctly reproduce the evolution of properties in time. From the results obtained from Table 1, this was done accurately for all properties considered, with temperature at Sines (station MS 1) buoy and salinity at Cadiz buoy (station MS 5) being the ones with lower MSS (0.63 and 0.31 respectively). Sines is located in a region of high variability regarding SST due to the seasonal upwelling events occurring at the west coast. Especially in the month of October where in general these mesoscale features are more intense, stronger bias may occur if the model doesn't completely reproduce these features. Regarding salinity results measured at station MS 5, although SOMA is underestimating the observed salinity during the validation period, when looking at the time evolution between model and observations (Fig. 4) they seem to follow a similar pattern, particularly until day 22 when the abrupt decrease in salinity was captured by the model. To understand this underestimation in salinity, and due to the location of station MS 5 being close to Level 1 boundary, SOMA forcing conditions provided by PCOMS were compared against station MS 5 salinity time series. Results obtained (MSS = 0.32 and RMSD = 0.20) show how boundary conditions may explain the error found. Time series for station MS 5 were also extracted from two operational systems in place for the study region (IBI-MFC and Mercator) to have an estimation of the relative magnitude of the error considered in SOMA. MSS values of 0.45 and 0.40 were found respectively for IBI-MFC and Mercator supporting the fact that salinity, unlike temperature, is still not very well resolved in global/regional models, mostly due to the availability of remote sensing data for assimilation. Although errors in salinity might be important near the boundary, inside the SOMA domain results from the different vertical profiles accessed during the validation show a good agreement between model and observations for both temperature and salinity.

SOMA current velocities validated at the surface (HF Radar), in depth (ADCP) and as a time series (Cadiz Buoy) with overall results showing good reproductions of the observed velocities. This is especially true when looking at the validation results obtained for the time series at Cadiz Buoy (Table 1), with MSS varying from 0.98 for the current velocity and 0.91 for the current direction (Fig. 4). Also, HF Radar results (Fig. 7) show that the model succeeds in reproducing the current field observed, and inclusively there is an improvement on the surface velocity with the increase in resolution from Level 1 to Level 2. While further validation is still required, using more available HF Radar data to capture the region variability, the results presented highlight the advantages of the downscalling methodology in coastal areas where the bathymetry gradients are important shaping mechanism of the current field. In depth, SOMA current velocity and direction was also validated to a good standard when compared with ADCP transect at both 35 m and 105 m depth.

4.2. Lagrangian model validation and CleanSeaNet backtracking results

To validate SOMA Lagrangian component, trajectories from satellite-tracked drifters with different timespans (2011 till 2013) were used to validate model results. Although not equivalent to a real oil spill, it is an available method to validate the simulated trajectories and estimate model errors that should integrate future forecasts for oil trajectories. The results achieved (depicted in Table 2) presented high *s* index values, fostering the need to perform two additional simulations, considering distinct scenarios, in order to understand and explain the differences obtained. The results are not fully conclusive, some drifters present lower *s* index values at 15 m depth (Drifter 4), some at the surface (Drifter 2), and some at the surface with 3% of the wind speed added (Drifter 5). Some drifters still, reflect minor changes in the three scenarios simulated (Drifter 1 and 3). As previously mentioned, inside the model domain, the circulation at the surface is mainly wind driven, particularly in the study area, known by its high mesoscale variability (Haynes et al., 1993; Peliz et al., 2002, 2005; Serra and Ambar, 2002; Torres et al., 2003; Relvas and Barton, 2005). This mesoscale variability was recognized as difficult to capture by the atmospheric model, possibly justifying the differences between drifters' trajectories and model results. Also, as mentioned above, testing redundant sources for hydrodynamic and atmospheric forcing is being considered, which can lead to improved validation results.

As suggested by Janeiro et al. (2014), the inclusion of Stokes drift may improve the results. To understand the impact of not considering the Stokes drift in the present study, wave hindcasts from an operational WW3 model for the North Atlantic with a 25 km resolution presently run at Hidromod were used. Sim 2 scenario (particles imposed at the surface) for Drifter 4 was re-run using the Stokes Drift formulation described in Fernandes et al. (2013). After 24 h the distance model-buoy obtained in the simulation considering the Stokes drift was 13 km with the s index being 0.82. This contrasts with the values 8 km and 0.69 previously found not considering this velocity component. Although in this case considering the Stokes drift seems to weaken the comparison with the drifter trajectory, the results show that it affects

significantly the Lagrangian particles and shouldn't be disregarded. A high resolution local wave model implementation is also a development being prepared and soon implemented in the operational system, with the potential of improving the results obtained.

Due to lack of availability data, SOMA Oil Module was not validated and we can't retrieve any conclusions regarding the evolution of oil-weathering processes, as none was considered in this work. Nonetheless, the methods implemented in MOHID Oil Module has been used in previous studies (e.g. Fernandes, 2001; Janeiro et al., 2008; Fernandes et al., 2013) with good results being achieved. Also, its successful application has been also on going in the scope of several European Framework Projects (e.g. ARCOPOL; ARGOMARINE). Still, site specific validation is required, especially for oil dispersion, and it is an activity planned.

The integration of remote oil spill detection techniques, backtracking methods and AIS data is of paramount importance in regions with high shipping traffic, hence higher probability of illegal discharges, such is the case of the study area. A robust methodology was applied using SOMA in hindcast mode to backtrack a CleanSeaNet detection southeast of Sagres. From results obtained, six ships had trajectories inside the search areas defined, but only four of them matched the selection criteria considered. A tanker trajectory was detected in the 12 h search radius, while three general cargo ships were detected in the 24, 36 and 48 h. The tanker detection occurred at the first search radius considered with radius and error quantified as 6.7 $\pm$ 4.8 km, respectively. The following detections had search radius and errors ranging from 15 $\pm$ 11.3 km (24 h) to 26.4 $\pm$ 19.8 (48 h). The quantified errors in the backtracking simulations reflect not only the errors from the numerical methods applied, but also include the uncertainty associated to the mesoscale variability of the region, captured in the different drifter trajectories used during the validation. This fact can explain the magnitude of the errors found when comparing them with the work of Abascal et al. (2012) where the authors, using HF Radar current fields in the backtrack simulations combined with dedicated drifter experiments in the day of the backtracking experiments, obtained errors of 1.0 $\pm$ 0.85 km after approximately 12 h backtrack, contrasting with the 6.7 $\pm$ 4.8 km obtained in this study. The work of Dominicis et al. (2013a), more comparable with the present study, where operational systems of increasing grid resolutions were used to validate the MEDSLIK oil model, presented errors more similar to the ones found with SOMA (4 km after 12 h and approximately 10 km after 24 h) when using the high resolution (2.2 km) hydrodynamic results from the Adriatic Forecasting System.

Although the differences presented are significant, especially when these values are translated in a radius for search area, the backtrack validation in this study is considered more realistic and comprehensive of the different oceanographic variability that characterize the South Iberian, making it suitable for oil pollution backtracking studies. The methodology applied also lead to the development of a time and space filter to select possible candidates to the pollution event based on AIS information. This tool was efficiently applied and tested with the detection of six boats, among them one tanker on the first search radius considered, which presented the higher confidence. While this is only a test of concept, the integration of these technologies allows heightening the monitoring and consequent protection of coastal environments, in a twofold: by assisting in identifying the source of the spill and discouraging illegal oil pollution.

5. Conclusions

SOMA was considered a validated operational system with the ability to forecast oil spill trajectories in the SW Iberian coast. Mesoscale features present in the region, observed and described by several authors, were clearly identified by observing the remote sensing SST data, with SOMA being able to reproduce these features to a good extend. Validation results pointed out for the model dependence on forcing conditions, where hydrodynamic and atmospheric forcing's are understood to have a regional importance due to the characteristic mesoscale activity of the region in study. Arises the need to test new operational forcing conditions with improved resolutions and upgraded data assimilation systems to minimize errors found in SOMA. The Stokes drift, not included in SOMA, was accessed and shown that it affects significantly the Lagrangian particles. SOMA wave component is under development and soon will be implemented and validated. Also, to include and validate oil weathering processes, especially oil dispersion, is a short-term activity to further access the suitability of the model to simulate these pollution events. Finally, the results obtained from the backtracking simulations were encouraging. A robust methodology was applied to derive possible pollution candidates from AIS positions, while incorporating model trajectory errors calculated during the validation procedure, thus minimizing the uncertainty due to the region oceanic and atmospheric variability. This is understood as paramount to provide useful information for the decision-making process related to oil pollution in the region.

Acknowledgments

This work was funded by a Doctoral grant, reference SFRH/BD/44850/2008, from the Fundação para a Ciência e Tecnologia and from the European Union's Horizon 2020 research and innovation programme under grant agreement 633211-AtlantOS to whom we would like to thank. Special thanks to Hidromod and to the Helenic National Meteorological Service for supplying in an operational way respectively, the hydrodynamic and atmospheric forcing conditions used in the system. For the calibration/validation procedure we would like to acknowledge the Coriolis project from most of the data used was retrieved, the Project IMPACT (Long-term effects of continued trawling on deep-water muddy grounds) a EU programme Eurofleets (www.eurofleets.eu) to Instituto Hidrográfico; to the Direção de Combate à Poluição do Mar and special thanks to Prof. Jorge Gonçalves from CCMAR.

References

Abascal, A.J., Castanedo, S., Mendez, F.J., Medina, R., Losada, I.J., 2009. Calibration of a Lagrangian transport model using drifting buoys deployed during the prestige oil spill. J. Coast. Res. 251:80–90. http://dx.doi.org/10.2112/07-0849.1.

Abascal, A.J., Castanedo, S., Fernández, V., Medina, R., 2012. Backtracking drifting objects using surface currents from high-frequency (HF) radar technology. Ocean Dyn. 62: 1073–1089. http://dx.doi.org/10.1007/s10236-012-0546-4.

Allen, C.M., 1982. Numerical simulation of contaminant dispersion in estuary flows. Proc. R. Soc. Lond. A381, 179–194.

Álvarez-Salgado, X.A., Figueiras, F., Pérez, F., Groom, S., Nogueira, E., Borges, A., Chou, L., Castro, C., Moncoiffé, G., Ríos, A., Miller, A.E., Frankignoulle, M., Savidge, G., Wollast, R., 2003. The Portugal coastal counter current off NW Spain: new insights on its biogeochemical variability. Prog. Oceanogr. 56:281–321. http://dx.doi.org/10.1016/S0079-6611(03)00007-7.

Ascione Kenov, I., Campuzano, F., Franz, G., Fernandes, R., Viegas, C., Sobrinho, J., de Pablo, H., Amaral, A., Pinto, L., Mateus, M., Neves, R., 2014. Advances in modeling of water quality in estuaries. In: Finkl, C.W., Makowski, C. (Eds.), Remote Sensing and Modeling. Springer International Publishing, pp. 237–276.

Balseiro, C.F., Carracedo, P., Gómez, B., Leitão, P.C., Montero, P., Naranjo, L., Penabad, E., Pérez-Muñuzuri, V., 2003. Tracking the prestige oil spill: an operational experience in simulation at MeteoGalicia. Weather 58 (12), 452–458.

Barron, C.N., Smedstad, L.F., Dastugue, J.M., Smedstad, O.M., 2007. Evaluation of ocean models using observed and simulated drifter trajectories: impact of sea surface height on synthetic profiles for data assimilation. J. Geophys. Res. Ocean. 112:1–11. http://dx.doi.org/10.1029/2006JC003982.

Bebiano, M.L., 1995. Effects of pollutants in the Ria Formosa lagoon, Portugal. Sci. Total Environ. 171:107–115. http://dx.doi.org/10.1016/0048-9697 (95)04672-9.

Blayo, E., Debreu, L., 2005. Revisiting open boundary conditions from the point of view of characteristic variables. Ocean Model 9, 231–252.

Blumberg, A.F., Kantha, L.H., 1985. Open boundary condition for circulation models. J. Hydraulic Eng. ASCE 111, 237–2555.

Broström, G., Carrasco, A., Hole, L.R., Dick, S., Janssen, F., Mattsson, J., Berger, S., 2011. Usefulness of high resolution coastal models for operational oil spill forecast: the "Full City" accident. Ocean Sci. 7:805–820. http://dx.doi.org/10.5194/os-7-805-2011.

Buchard, H., Bolding, K., Villarreal, M.R., 1999. GOTM, a General Ocean Turbulence Model. Theory, implmentation and test cases. Report EUR18745 EN, European Comission (103 pp.).

Caballero, A., Espino, M., Sagarminaga, Y., Ferrer, L., Uriarte, A., González, M., 2008. Simulating the migration of drifters deployed in the Bay of Biscay, during the prestige crisis. Mar. Pollut. Bull. 56:475–482. http://dx.doi.org/10.1016/j.marpolbul.2007.11.005.

Campuzano, F.J., Kenov, I., Brito, D., Juliano, M., Fernandes, R., Pinto, L., Neves, R., 2014. Numerical evaluation of the river nutrients for the Western Iberian coastal region. 3 Jornadas Da Engenharia Hidrográfica. Instituto Hidrográfico, Lisbon, Portugal, pp. 263–266.

Canuto, V.M., Howard, A., Cheng, Y., Dubovikov, M.S., 2001. Ocean turbulence. part I: one-point closure model—momentum and heat vertical diffusivities. J. Phys. Oceanogr. 31: 1413–1426. http://dx.doi.org/10.1175/1520-0485(2001)031<1413:OTPIOP>2.0.CO;2.

Direção Geral de Energia e Geologia (DGEG), 2014. Política dos Recurso Geológicos - Petróleo. WWW Page. http://www.dgeg.pt.

Dominicis, M. De, Pinardi, N., Zodiatis, G., Archetti, R., De Dominicis, M., Pinardi, N., Zodiatis, G., Dominicis, M. De, 2013a. MEDSLIK-II, a Lagrangian marine oil spill model for short-term forecasting – part 1: theory. Geosci. Model Dev. 6:1949–1997. http://dx.doi.org/10.5194/gmdd-6-1949-2013.

Dominicis, M. De, Pinardi, N., Zodiatis, G., Archetti, R., De Dominicis, M., 2013b. MEDSLIK-II, a Lagrangian marine surface oil spill model for short-term forecasting — part 2: numerical simulations and validations. Geosci. Model Dev. 6:1999–2043. http://dx.doi.org/10.5194/gmdd-6-1999-2013.

European Maritime Safety Agency (EMSA), 2014. Addressing illegal discharges in the marine environment (100 pp.).

Fernandes, R., 2001. Modelação de derrames de Hidrocarbonetos. IST - Universidade Técnica de Lisboa.

Fernandes, R., Neves, R., Viegas, C., Leitão, P., 2013. Integration of an oil and inert spill model in a framework for risk management of spills at sea—a case study for the Atlantic area. 37th AMOP Technical Seminar on Environmental Contamination and Response, p. 28.

García-Lafuente, J., Delgado, J., Criado-Aldeanueva, F., Bruno, M., del Río, J., Miguel Vargas, J., 2006. Water mass circulation on the continental shelf of the Gulf of Cádiz. Deep Sea Res. Part II Top. Stud. Oceanogr. 53:1182–1197. http://dx.doi.org/10.1016/j.dsr2.2006.04.011.

Gouveia, J.A.V., Guedes Soares, C., Soares, C., Guedes Soares, C., 2010. Oil spill incidents in Portuguese waters. Advanced Ship Design for Pollution Prevention. Taylor & Francis Group, London, UK:pp. 217–223 http://dx.doi.org/10.1201/b10565-27.

Haynes, R., Barton, E., Pilling, I., 1993. Development, persistence, and variability of upwelling filaments off the Atlantic coast of the Iberian Peninsula. J. Geophys. Res. 98 (C12), 22681–22692.

Janeiro, J., Fernandes, E., Martins, F., Fernandes, R., 2008. Wind and freshwater influence over hydrocarbon dispersal on Patos lagoon. Brazil. Mar. Pollut. Bull. 56:650–665. http://dx.doi.org/10.1016/j.marpolbul.2008.01.011.

Janeiro, J., Martins, F., Relvas, P., 2012. Towards the development of an operational tool for oil spills management in the Algarve coast. J. Coast. Conserv. 16:449–460. http://dx.doi.org/10.1007/s11852-012-0201-8.

Janeiro, J., Zacharioudaki, A., Sarhadi, E., Neves, A., Martins, F., 2014. Enhancing the management response to oil spills in the Tuscany archipelago through operational modelling. Mar. Pollut. Bull. 85:574–589. http://dx.doi.org/10.1016/j.marpolbul.2014.03.021.

Kallos, G., 1997. The Regional weather forecasting system SKIRON. Proceedings, Symposium on Regional Weather Prediction on Parallel Computer Environments Athens, Greece (9 pp.).

Leitão, P., Coelho, H., Santos, A., Neves, R., 2005. Modelling the main features of the Algarve coastal circulation during July 2004: a downscaling approach. J. Atmos. Ocean Sci. 10:421–462. http://dx.doi.org/10.1080/17417530601127704.

Liu, Y., Weisberg, R.H., 2011. Evaluation of trajectory modeling in different dynamic regions using normalized cumulative Lagrangian separation. J. Geophys. Res. 116: 1–13. http://dx.doi.org/10.1029/2010JC006837.

Mateus, M., Riflet, G., Chambel, P., Fernandes, L., Fernandes, R., Juliano, M., Campuzano, F., de Pablo, H., Neves, R., 2012. An operational model for the West Iberian coast: products and services. Ocean Sci. 8:713–732. http://dx.doi.org/10.5194/os-8-713-2012.

Martins, F., Leitão, P., Silva, A., 2001. 3D modelling in the sado estuary using a new generic vertical discretization approach. Oceanol. Acta 24:S51–S62. http://dx.doi.org/10.1016/S0399-1784(01)00092-5.

Martinsen, E.A., Engedahl, H., 1987. Implementation and testing of a lateral boundary scheme as an open boundary condition in a barotropic ocean model. Coast. Eng. 11: 603–627. http://dx.doi.org/10.1016/0378-3839(87)90028-7.

NASA, 2014. National Aeronautics and Space Administration. http://oceancolor.gsfc.nasa.gov/ Accessed 25/06/2014.

O'Donncha, F., Hartnett, M., Nash, S., Ren, L., Ragnoli, E., 2015. Characterizing observed circulation patterns within a bay using HF radar and numerical model simulations. J. Mar. Syst. 142:96–110. http://dx.doi.org/10.1016/j.jmarsys.2014.10.004.

Oliveira, P.B., Peliz, Á., Dubert, J., Rosa, T.L., Santos, A.M.P., 2004. Winter geostrophic currents and eddies in the Western Iberia coastal transition zone. Deep Sea Res. Part I Oceanogr. Res. Pap. 51:367–381. http://dx.doi.org/10.1016/j.dsr.2003.10.016.

OSI SAF, 2013. EUMETSAT OSI SAF. http://www.osi-saf.org/ Accessed 15/04/2013.

Papadopoulos, A., Katsafados, P., Kallos, G., Nickovic, S., 2001. The Weather Forecasting System for Poseidon - an Overview. Glob. Atmos. Ocean Syst. 8 (2–3):219–237. http://dx.doi.org/10.1080/10236730260151201.

Peliz, Á., Rosa, T.L., Santos, A.M.P., Pissarra, J.L., 2002. Fronts, jets, and counter-f lows in the Western Iberian upwelling system. J. Mar. Syst. 35, 61–77.

Peliz, Á., Dubert, J., Santos, A.M.P., Oliveira, P.B., Le Cann, B., 2005. Winter upper ocean circulation in the Western Iberian Basin—fronts, Eddies and Poleward flows: an overview. Deep Sea Res. Part I Oceanogr. Res. Pap. 52:621–646. http://dx.doi.org/10.1016/j.dsr.2004.11.005.

Peliz, A., Marchesiello, P., Santos, A.M.P., Dubert, J., Teles-Machado, A., Marta-Almeida, M., Le Cann, B., 2009. Surface circulation in the Gulf of Cadiz: 2. Inflow-outflow coupling and the Gulf of Cadiz slope current. J. Geophys. Res. 114:C03011. http://dx.doi.org/10.1029/2008JC004771.

Pires, A., Nolasco, R., Rocha, A., Dubert, J., 2013. Assessing future climate change in the Iberian upwelling system. J. Coast. Res.:1909–1914 http://dx.doi.org/10.2112/SI65-323.1.

Price, J.D., Bush, M.R., 2004. Comparisons between model forecast and observed boundary layer profiles and related comments on cloud prediction. Weather Forecast. 19: 959–969. http://dx.doi.org/10.1175/822.1.

Price, J., Reed, M., Howard, M., Johnson, W., Ji, Z., Marshall, C., Guinassojr, N., Rainey, G., 2006. Preliminary assessment of an oil-spill trajectory model using satellite-tracked, oil-spill-simulating drifters. Environ. Model. Softw. 21:258–270. http://dx.doi.org/10.1016/j.envsoft.2004.04.025.

Relvas, P., Barton, E.D., 2005. A separated jet and coastal counterflow during upwelling relaxation off Cape São Vicente (Iberian Peninsula). Cont. Shelf Res. 25:29–49. http://dx.doi.org/10.1016/j.csr.2004.09.006.

Relvas, P., Barton, E.D.D., Dubert, J., Oliveira, P.B., Peliz, A., da Silva, J.C.B., Santos, A.M.P., Silva, J.C.B., Santos, A.M.P., 2007. Physical oceanography of the Western Iberia ecosystem: latest views and challenges. Prog. Oceanogr. 74:149–173. http://dx.doi.org/10.1016/j.pocean.2007.04.021.

Santos, F., Gómez-Gesteira, M., DeCastro, M., Álvarez, I., Res, C., 2011. Upwelling along the Western coast of the Iberian Peninsula: dependence of trends on fitting strategy. Clim. Res. 48:213–218. http://dx.doi.org/10.3354/cr00972.

Serra, N., Ambar, I., 2002. Eddy generation in the Mediterranean undercurrent. Deep. Res. Part II Top. Stud. Oceanogr. 49:4225–4243. http://dx.doi.org/10.1016/S0967-0645(02)00152-2.

Silveira, P.A.M., Teixeira, A.P., Soares, C.G., 2013. Use of AIS data to characterise marine traffic patterns and ship collision risk off the coast of Portugal. J. Navig. 66:879–898. http://dx.doi.org/10.1017/S0373463313000519.

Sotillo, M.G., Fanjul, E.A., Castanedo, S., Abascal, A.J., Menendez, J., Emelianov, M., Olivella, R., García-Ladona, E., Ruiz-Villarreal, M., Conde, J., Gómez, M., Conde, P., Gutierrez, A.D., Medina, R., 2008. Towards an operational system for oil-spill forecast over Spanish waters: initial developments and implementation test. Mar. Pollut. Bull. 56: 686–703. http://dx.doi.org/10.1016/j.marpolbul.2007.12.021.

Teles-Machado, A., Peliz, Á., Dubert, J., Sánchez, R.F., 2007. On the onset of the Gulf of Cadiz coastal countercurrent. Geophys. Res. Lett. 34:1–5. http://dx.doi.org/10.1029/2007GL030091.

Thompson, K.R., 2003. Prediction of surface currents and drifter trajectories on the inner Scotian shelf. J. Geophys. Res. 108:1–10. http://dx.doi.org/10.1029/2001JC001119.

Torres, R., Barton, E.D., Miller, P., Fanjul, E., 2003. Spatial patterns of wind and sea surface temperature in the Galician upwelling region. J. Geophys. Res. 108:1–14. http://dx.doi.org/10.1029/2002JC001361.

Umlaut, L., Burchard, H., 2005. Second-order turbulence closure models for geophysical boundary layers. A review of recent work. Cont. Shelf Res. 25:725–827. http://dx.doi.org/10.1016/j.csr.2004.08.004.

Verjovkina, S., Raudsepp, U., Kõuts, T., Vahter, K., 2010. Validation of seatrack web using surface drifters in the Gulf of Finland and Baltic Proper. 2010 IEEE/OES US/EU Baltic International Symposium. Riga, Latvia, pp. 1–8.

Willmott, C., 1981. On the validation of models. Phys. Geogr. 2 (C5), 184–194.

Zodiatis, G., Lardner, R., Solovyov, D., Panayidou, X., De Dominicis, M., 2012. Predictions for oil slicks detected from satellite images using MyOcean forecasting data. Ocean Sci. Discuss. 9:1973–2000. http://dx.doi.org/10.5194/osd-9-1973-2012.